

Ground state properties and potential energy surfaces of ^{270}Hs from multidimensionally-constrained relativistic mean field model

Xu MENG^{1,2}, Bing-Nan LU³, and Shan-Gui ZHOU^{1,2,4,5*}

¹CAS Key Laboratory of Theoretical Physics, Institute of Theoretical Physics, Chinese Academy of Sciences, Beijing 100190, China;

²School of Physical Sciences, University of Chinese Academy of Sciences, Beijing 100049, China;

³Facility for Rare Isotope Beams and Department of Physics and Astronomy, Michigan State University, MI 48824, USA;

⁴Center of Theoretical Nuclear Physics, National Laboratory of Heavy Ion Accelerator, Lanzhou 730000, China;

⁵Synergetic Innovation Center for Quantum Effects and Application, Hunan Normal University, Changsha 410081, China

Received April 22, 2019; accepted April 30, 2019; published online October 8, 2019

We study the ground state properties, potential energy curves and potential energy surfaces of the superheavy nucleus ^{270}Hs by using the multidimensionally-constrained relativistic mean-field model with the effective interaction PC-PK1. The binding energy, size and shape as well as single particle shell structure corresponding to the ground state of this nucleus are obtained. ^{270}Hs is well deformed and exhibits deformed doubly magic feature in the single neutron and proton level schemes. One-dimensional potential energy curves and two-dimensional potential energy surfaces are calculated for ^{270}Hs with various spatial symmetries imposed. We investigate in detail the effects of the reflection asymmetric and triaxial distortions on the fission barrier and fission path of ^{270}Hs . When the axial symmetry is imposed, the reflection symmetric and reflection asymmetric fission barriers both show a double-hump structure and the former is higher. However, when triaxial shapes are allowed the reflection symmetric barrier is lowered very much and then the reflection symmetric fission path becomes favorable.

MDC-RMF model, superheavy nuclei, potential energy surface, fission barrier, reflection asymmetry, triaxial deformation

PACS number(s): 21.10.-k, 21.60.Jz, 27.90.+b, 23.70.+j

Citation: Meng X, Lu B N and Zhou S G, Ground state properties and potential energy surfaces of ^{270}Hs from multidimensionally-constrained relativistic mean field model, *Sci. China-Phys. Mech. Astron.* **63**, 212011 (2020), doi: 10.1007/s11433-019-9422-1

1 Introduction

Exploration of the charge and mass limits of atomic nuclei is at the forefront of modern nuclear physics research [1-3]. When described as charged liquid drops, nuclei with $Z \geq 104$ would not exist because the fission barriers would disappear. Quantum shell effects may cause additional binding in some of these nuclei. Consequently, the existence of an “island of stability” of superheavy nuclei (SHN) was predicted in 1960s because of this extra binding [4-9]. Since then, study on SHN has progressed very much. Until now, superheavy elements (SHE) with $Z \leq 118$ have been synthesized [10-12].

However, the island is still not located and various predictions of its center have been made [4-9, 13-20]. Contrary to the fact that the island of stability is very elusive and the predicted centers of this island are far beyond the current experimental ability, the existence of a “shallow” of SHN, which is closer to the continent of stable nuclei, has been theoretically and experimentally well established. This shallow was predicted to comprise deformed SHN and to be centered around $Z = 108$ and $N = 162$ [21-25]. Many SHN on the shallow have been synthesized, including $^{270}_{108}\text{Hs}_{162}$ [26, 27]. The deformed doubly magic SHN ^{270}Hs sitting at the center of the shallow has become one of the most important examples for the study on the structure and fission properties of SHN.

*Corresponding author (email: sgzhou@itp.ac.cn)

Study on the ground state and fission barrier is essential in learning the stability properties, decay and fission dynamics of SHN. Although the most relevant shape degree of freedom involved in nuclear fission is the axial quadrupole deformation β_{20} corresponding to the elongation of the whole nucleus along its symmetry axis, other shape degrees of freedom may also play crucial roles during the fission process [28–40]. Therefore examining the multidimensional potential energy surfaces (PESs) for a nucleus in question is important for obtaining detailed information about the fission properties.

We have developed multidimensionally-constrained (MDC) covariant density functional theories (CDFTs) to calculate and study PESs for SHN and heavy nuclei [37, 39–41]. In these theories, the shape degrees of freedom $\beta_{\lambda\mu}$ with μ being even numbers are self-consistently included, such as β_{20} , β_{22} , β_{30} , β_{32} , β_{40} , β_{42} and β_{44} . Either the BCS approach or the Bogoliubov transformation has been implemented for considering pairing correlations. The MDC-CDFT with the BCS approach used for treating pairing correlations is known as the MDC relativistic mean field (RMF) model, whereas that with the Bogoliubov transformation is known as the MDC relativistic Hartree–Bogoliubov (RHB) model. The MDC-RMF model has been used to investigate fission barriers and PESs of actinide nuclei; in particular, a three-dimensional PES has been obtained for ^{240}Pu [37, 39]. It was found that besides the reflection asymmetric octupole shape, the triaxial deformation plays a crucial role on the second fission barriers in actinide nuclei.

In this work, we use the MDC-RMF model to study the ground state properties and PESs of the doubly magic deformed nucleus ^{270}Hs . This is the first thorough study on SHN with MDC-CDFTs. We present the first PES for ^{270}Hs considering both triaxiality and reflection asymmetry. The remainder of this paper is organized as follows. The MDC-RMF model will be introduced in section 2. The results and discussions are presented in section 3. Finally in section 4, we will summarize this study and provide some perspectives on the study on SHN with MDC-CDFTs.

2 The multidimensionally-constrained relativistic mean field model

CDFT is one of the most successful self-consistent approaches which has been extensively used to study the properties of atomic nuclei throughout the nuclear chart [42–52]. The formalism and applications of the CDFT can be found in Ref. [52]. The details of the MDC-CDFTs have been given in Refs. [39–41]. For completeness, here we present briefly the formalism of MDC-CDFTs.

In the CDFT, a nucleus is described to be a composite of A nucleons which interact through the exchanges of mesons and photons or contact interactions (point-couplings). In this paper we focus on the CDFT with nonlinear point couplings (NL-PC). The time-reversal symmetry is assumed for nuclei in question.

The NL-PC Lagrangian reads,

$$\mathcal{L} = \bar{\psi}(i\gamma_{\mu}\partial^{\mu} - M)\psi - \mathcal{L}_{\text{lin}} - \mathcal{L}_{\text{nl}} - \mathcal{L}_{\text{der}} - \mathcal{L}_{\text{Cou}}, \quad (1)$$

where the linear, nonlinear and derivative coupling terms and the Coulomb term are given respectively as follows,

$$\mathcal{L}_{\text{lin}} = \frac{1}{2}\alpha_S\rho_S^2 + \frac{1}{2}\alpha_V\rho_V^2 + \frac{1}{2}\alpha_{TS}\vec{\rho}_{TS}^2 + \frac{1}{2}\alpha_{TV}\vec{\rho}_{TV}^2, \quad (2)$$

$$\mathcal{L}_{\text{nl}} = \frac{1}{3}\beta_S\rho_S^3 + \frac{1}{4}\gamma_S\rho_S^4 + \frac{1}{4}\gamma_V[\rho_V^2]^2, \quad (3)$$

$$\mathcal{L}_{\text{der}} = \frac{1}{2}\delta_S[\partial_V\rho_S]^2 + \frac{1}{2}\delta_V[\partial_V\rho_V]^2 + \frac{1}{2}\delta_{TS}[\partial_V\vec{\rho}_{TS}]^2 + \frac{1}{2}\delta_{TV}[\partial_V\vec{\rho}_{TV}]^2, \quad (4)$$

$$\mathcal{L}_{\text{Cou}} = \frac{1}{4}F^{\mu\nu}F_{\mu\nu} + e\frac{1-\tau_3}{2}A_0\rho_V. \quad (5)$$

M is the nucleon mass and α_S , α_V , α_{TS} , α_{TV} , β_S , γ_S , γ_V , δ_S , δ_V , δ_{TS} and δ_{TV} are the coupling constants in different channels. ρ_S and $\vec{\rho}_{TS}$ are the isoscalar and isovector densities; ρ_V and $\vec{\rho}_{TV}$ are the time-like components of isoscalar and isovector currents.

Applying the mean field and no sea approximations, the Dirac equation for nucleons is derived with the Slater determinant used as the trial wave function,

$$\hat{h}\psi_k(\mathbf{r}) = \epsilon_k\psi_k(\mathbf{r}), \quad (6)$$

where

$$\hat{h} = \boldsymbol{\alpha} \cdot \mathbf{p} + \beta[M + S(\mathbf{r})] + V(\mathbf{r}). \quad (7)$$

The scalar potential $S(r)$ and vector potential $V(r)$ are determined by the various scalar and vector densities given in Eqs. (2–5).

One can solve the Dirac equation in several different harmonic oscillator bases [53–60]. In the MDC-CDFTs, an axially deformed harmonic oscillator (ADHO) basis [53, 54] is used to expand the single particle Dirac wave functions. The ADHO basis consists of the eigenstates of the Schrödinger equation,

$$\left[-\frac{\hbar^2}{2M}\nabla^2 + V_B(z, \rho) \right] \Phi_{\alpha}(\mathbf{r}\sigma) = E_{\alpha}\Phi_{\alpha}(\mathbf{r}\sigma), \quad (8)$$

where $\mathbf{r} = (z, \rho)$ with $\rho = \sqrt{x^2 + y^2}$ and

$$V_B(z, \rho) = \frac{1}{2}M(\omega_{\rho}^2\rho^2 + \omega_z^2z^2), \quad (9)$$

is the ADHO potential with ω_ρ (ω_z) being the oscillator frequency perpendicular to (along) the symmetry axis. The solution of Eq. (8) is obtained as

$$\Phi_\alpha(\mathbf{r}\sigma) = C_\alpha \phi_{n_z}(z) R_{n_\rho}^{m_l}(\rho) \frac{1}{\sqrt{2\pi}} e^{im_l\varphi} \chi_{m_s}(\sigma), \quad (10)$$

where a complex number C_α is introduced for convenience. χ_{m_s} is a two-component spinor. $\phi_{n_z}(z)$ and $R_{n_\rho}^{m_l}(\rho)$ are the harmonic oscillator wave functions,

$$\phi_{n_z}(z) = \frac{1}{\sqrt{b_z}} \frac{1}{\pi^{1/4} \sqrt{2^{n_z} n_z!}} H_{n_z} \left(\frac{z}{b_z} \right) e^{-z^2/2b_z}, \quad (11)$$

$$R_{n_\rho}^{m_l}(\rho) = \frac{1}{b_\rho} \sqrt{\frac{2n_\rho!}{(n_\rho + |m_l|)!}} \left(\frac{\rho}{b_\rho} \right)^{|m_l|} \times L_{n_\rho}^{|m_l|} \left(\frac{\rho^2}{b_\rho^2} \right) e^{-\rho^2/2b_\rho^2}. \quad (12)$$

The oscillator lengths b_z and b_ρ are related to the frequencies as $b_z = 1/\sqrt{M\omega_z}$ and $b_\rho = 1/\sqrt{M\omega_\rho}$.

These basis states are eigenstates of \hat{j}_z with eigenvalues $K_\alpha = m_l + m_s$. The deformation of the basis β_{basis} is defined through the relations $\omega_z = \omega_0 \exp(-\sqrt{5/4\pi}\beta_{\text{basis}})$ and $\omega_\rho = \omega_0 \exp(\sqrt{5/16\pi}\beta_{\text{basis}})$, where $\omega_0 = (\omega_z \omega_\rho^2)^{1/3}$ is the frequency of the corresponding spherical oscillator potential.

When solving the RMF equations, the Dirac spinor is expanded in terms of the complete basis $\{\Phi_\alpha(\mathbf{r}\sigma)\}$ as,

$$\psi_i(\mathbf{r}\sigma) = \begin{pmatrix} \sum_\alpha f_i^\alpha \Phi_\alpha(\mathbf{r}\sigma) \\ \sum_\alpha g_i^\alpha \Phi_\alpha(\mathbf{r}\sigma) \end{pmatrix}, \quad (13)$$

where $\alpha = \{n_z, n_\rho, m_l, m_s\}$ and f_i^α and g_i^α are the expansion coefficients to be determined. Following Ref. [61], the ADHO basis is truncated with $[n_z/f_z + (2n_\rho + |m_l|)/f_\rho] \leq N_f$ for the upper (large) component of the Dirac spinor where $f_z = \max(b_z/b_0, 1)$ and $f_\rho = \max(b_\rho/b_0, 1)$ are constants and $b_0 = 1/\sqrt{M\omega_0}$ is the spherical harmonic oscillator length. For the expansion of the lower (small) component of the Dirac spinor, the truncation of $N_g = N_f + 1$ is made to avoid the numerical instability.

In the MDC-CDFTs, we assume that the nuclear potentials and densities are invariant under the following operations: the reflection with respect to the y - z plane (\hat{S}_x), the reflection with respect to the x - z plane (\hat{S}_y) and the rotation of 180° with respect to the z axis (\hat{S}), i.e.,

$$\hat{S}_x \phi(x, y, z) = \phi(-x, y, z), \quad (14)$$

$$\hat{S}_y \phi(x, y, z) = \phi(x, -y, z), \quad (15)$$

$$\hat{S} \phi(x, y, z) = \phi(-x, -y, z). \quad (16)$$

These three operations and the identity \hat{I} form the V_4 group.

The pairing correlations are crucial in open shell nuclei. It has been shown that fission barriers are influenced very much by the pairing correlations [62]. In the MDC-RMF model [39], we employed the BCS approach with a separable pairing force of finite-range [63-65].

To obtain a PES, i.e., the energy of a nucleus as a function of various shape degrees of freedom $E = E(\{\beta_{\lambda\mu}\})$, one can perform constraint calculations [66]. A modified linear constraint method has been proposed [37, 39] in which the Routhian is calculated as,

$$E' = E_{\text{RMF}} + \sum_{\lambda\mu} \frac{1}{2} C_{\lambda\mu} Q_{\lambda\mu}. \quad (17)$$

In the $(n+1)$ th iteration, the variable $C_{\lambda\mu}$ is determined by,

$$C_{\lambda\mu}^{(n+1)} = C_{\lambda\mu}^{(n)} + k_{\lambda\mu} (\beta_{\lambda\mu}^{(n)} - \beta_{\lambda\mu}), \quad (18)$$

where $\beta_{\lambda\mu}$ is the desired deformation, $k_{\lambda\mu}$ is a constant and $C_{\lambda\mu}^{(n)}$ is the value in the n th iteration.

The RMF equations are solved iteratively. After a desired accuracy is achieved, we can calculate various physical quantities. For example, the intrinsic multipole moments are calculated from the density by

$$Q_{\lambda\mu} = \int d^3r \rho_V(\mathbf{r}) r^\lambda Y_{\lambda\mu}(\Omega), \quad (19)$$

where $Y_{\lambda\mu}(\Omega)$ is the spherical harmonics. The deformation parameter $\beta_{\lambda\mu}$ is obtained from the corresponding multipole moment by

$$\beta_{\lambda\mu} = \frac{4\pi}{3nR^4} Q_{\lambda\mu}, \quad (20)$$

where $R = r_0 A^{1/3}$ is the radius of the nucleus, the parameter $r_0 = 1.2$ fm and n represents proton, neutron or nucleon numbers Z , N or A . Applying the operations Eqs. (14-16) to the densities, one gets under the assumption of the V_4 symmetry,

$$\beta_{\lambda\mu} = \beta_{\lambda\bar{\mu}} = (-1)^\mu \beta_{\lambda\bar{\mu}}. \quad (21)$$

Therefore $\beta_{\lambda\mu} = 0$ when μ is an odd number. Consequently, the four deformations of the lowest order allowed in the MDC-RMF model are β_{20} , β_{22} , β_{30} and β_{32} .

The MDC-CDFTs have been applied to the study on fission barriers and PESs of actinide nuclei [37, 39], the third minima in PESs of light actinides [67], the non-axial octupole Y_{32} correlations in $N = 150$ isotones [68] and Zr isotopes [41], axial octupole correlations in $M\chi D$ [69] and Ba isotopes [70] and shapes of hypernuclei [71, 72]. Based on the PESs from MDC-CDFTs, the dynamics of spontaneous and induced fissions in actinide nuclei has been studied [73-76]. In this work, the MDC-RMF model is used to make the first thorough study on SHN, namely, the ground state properties and PESs of the doubly magic deformed nucleus ^{270}Hs .

3 Results and discussions

3.1 Numerical details

As mentioned in section 2, a truncation $[n_z/f_z + (2n_p + |m_l|)/f_\rho] \leq N_f$ is made on the ADHO basis. When studying the ground state properties and one-dimensional potential energy curves (PECs), we choose $N_f = 20$. Such a truncation is also made when the two-dimensional PESs are calculated with the axial symmetry imposed. For the two-dimensional PESs with both triaxial and reflection asymmetric deformations considered, a smaller basis with $N_f = 16$ is adopted because of the limitation of computational capabilities. We have checked that in the deformation range we are interested in, $N_f = 20$ (16) can give an accuracy of 0.1 (0.5) MeV in the total binding energy. Generally speaking, such accuracies warrant the conclusions drawn in this work concerning the effects of the reflection asymmetric and triaxial deformations on the fission barriers and fission paths of ^{270}Hs .

In the particle-hole (ph) channel, we use the effective interaction PC-PK1 which was determined by fitting to observables of 60 selected spherical nuclei including binding energies, charge radii and empirical pairing gaps [77]. As reviewed in Ref. [78], this empirical functional has been very successful in describing nuclear ground state properties, e.g., the Coulomb displacement energies between mirror nuclei [79], nuclear binding energies [80-82] and quadrupole moments [83-85] and phase transitions in the nuclear shape [86], and low-energy excited states including nuclear chiral rotations [87] and magnetic and antimagnetic rotations [88-92]. PC-PK1 has also been used to study properties of SHN [93-95].

In the separable pairing force of finite range used in the particle-particle (pp) channel, there are two parameters, the pairing strength G and the effective range of the pairing force a . They have been fixed by reproducing the density dependence of the pairing gap of symmetric nuclear matter at the Fermi surface calculated with the Gogny force D1S: $G = G_0 = 728 \text{ MeV}\cdot\text{fm}^3$ and $a = 0.644 \text{ fm}$ [64, 96]. In the present work, a fine-tuning of the pairing strength G has been made and $G/G_0 = 1.1$ is used which can reproduce the odd-even mass staggering of $N = 162$ isotones and Hs isotopes.

3.2 Ground state properties of ^{270}Hs

As a typical doubly magic deformed nucleus in the super-heavy mass region, ^{270}Hs has been studied extensively and many of the studies focused on the ground state properties. In Table 1 our results for the bulk properties of the ground state, including the binding energy E_B , deformation parameter β_2 and root mean square (rms) charge radius R_c , are compared with results from other models as well as the empirical

value from the latest ‘‘Atomic Mass Evaluation’’ (AME2016) [97-99].

Table 1 Ground state properties, including the binding energy E_B , deformation parameter β_2 and rms charge radius R_c , obtained from the MDC-RMF model. Results from other models and AME2016 are included for comparison. See text for more details.

Model	E_B (MeV)	β_2	R_c (fm)
MDC-RMF (PC-PK1)	1967.40	0.261	6.167
AME2016 [97-99]	1969.65		
MMM [24]	1969.20	0.229	
RMF (TMA) [100, 101]	1971.80	0.22	6.152
RMF (NLZ2) [100, 101]	1969.22	0.274	6.251
RMF (TMA) [102, 103]	1971.93	0.222	6.142
HFB-24 [104]	1968.45	0.26	
RMF (NL3) [105]	1974	0.26	
WS4 [106]	1970.27	0.217	
FRDM (2012) [107]	1971.48	0.222	
RCHB (PC-PK1) [82] ¹⁾	1952.65		6.132
RCHB (PC-PK1) + RBF [108] ²⁾	1969.20		6.132

¹⁾ In Ref. [82], the spherical symmetry is assumed for all nuclei.

²⁾ In Ref. [108], the RBF approach was applied to nuclear masses but not to charge radii predicted by the RCHB model in Ref. [82].

The ground state binding energy E_B of ^{270}Hs from our MDC-RMF model calculation is 1967.40 MeV. There is no experimental value for the binding energy of ^{270}Hs and in AME2016 $E_B = 1969.65 \text{ MeV}$ was derived from the trends in the mass surface (TMS) [97-99]. Our calculation result is very close to this value. In fact, almost all mass models, including the RMF models with various effective interactions [100-103, 105], the Skyrme Hartree-Fock-Bogoliubov mass model (HFB-24) [104], and the three typical macroscopic-microscopic models (MMM)—the one by Patyk et al. [24], the Weizsäcker-Skyrme model [109-111] (WS4 [106]) and the finite range droplet model [FRDM (2012)] [107], predicted similar E_B values as is seen in Table 1. The only exception is the relativistic continuum Hartree-Bogoliubov (RCHB) model [112-114] which has been used to study how the continuum effects can extend the nuclear chart [82, 115]. The binding energy calculated for ^{270}Hs from this model is 1952.65 MeV [82] which is much smaller than those from other model predictions and the empirical value from AME2016. The reason is that in the RCHB model, the spherical symmetry is assumed for all nuclei and this is certainly not true for ^{270}Hs . However, it is interesting to see that the radial basis function (RBF) approach [116-119] can eliminate local systematic deviations between the experimental mass values and those calculated from the RCHB model, thus improving very much the predictive power of the RCHB model for nuclear masses [108]. For ^{270}Hs , the binding energy from the RCHB+RBF approach is 1969.20 MeV which is fairly close

to the AME2016 value as well as other model predictions. Note that a deformed relativistic Hartree–Bogoliubov model in continuum (the DRHBc model) has been developed and used to study the deformation and continuum effects in exotic nuclei [120–123]. An international collaboration is working on producing a new chart of nuclides and a new mass table with the DRHBc model [124].

There are no experimental information on the quadrupole moment and deformation parameter β_2 for ^{270}Hs . From all model calculations with the deformation considered, ^{270}Hs is well deformed in the ground state. From our MDC-RMF calculation, the quadrupole deformations of the ground state of ^{270}Hs are $\beta_{20} = 0.261$ and $\beta_{22} = 0$, meaning that $\beta_2 = 0.261$. This β_2 value is quite similar to the results from HFB-24 and RMF model calculations with NLZ2 and NL3, but is larger than the RMF results with TMA and MMMs. While in the MDC-RMF model the reflection asymmetric shapes are allowed, the calculated octupole deformation $\beta_{30} = 0$ for the ground state of ^{270}Hs . The calculated hexadecupole deformation $\beta_{40} = -0.056$ which is comparable to $\beta_{40} = -0.04$ from HFB-24 [104], $\beta_{40} = -0.052$ from WS4 [106] and $\beta_{40} = -0.079$ from the FRDM (2012) [107]. The rms charge radius R_c has not been measured for ^{270}Hs . All calculations including ours give predictions of R_c values between 6.13 fm and 6.26 fm. Note that in Ref. [108], the RBF approach was not applied to the charge radii obtained from the RCHB calculations.

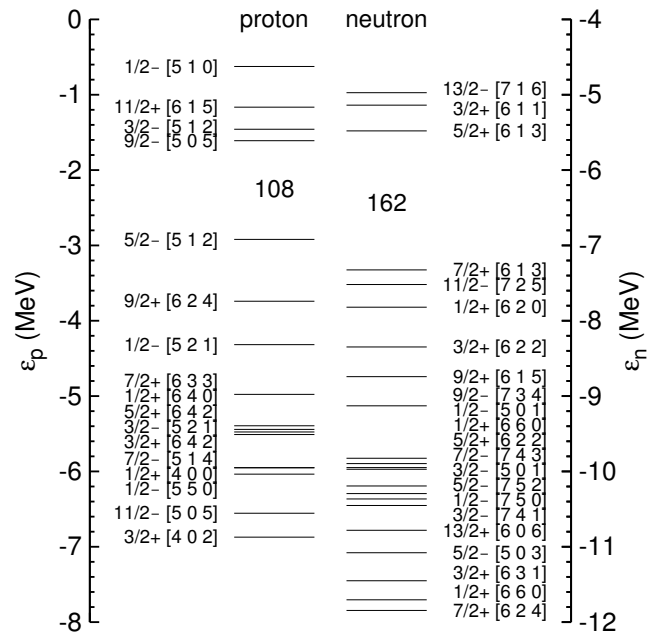


Figure 1 (Color online) Single proton and neutron levels of the ground state of ^{270}Hs . The Nilsson quantum numbers are given for each level.

Single proton and neutron energy levels of ^{270}Hs in the ground state are shown in Figure 1. Since ^{270}Hs is an axially

deformed nucleus with the reflection symmetry, we can label each single particle level with the Nilsson quantum numbers. In Figure 1, one can see clearly the feature of the double magicity. The shell gap is 1.3 MeV for protons at $Z = 108$ and around 2 MeV for neutrons at $N = 162$. Such gaps are very prominent considering the fact that in the superheavy region the single particle level density is quite large and grows faster than expected from the $A^{1/3}$ scaling even for spherical SHN [94]. In Ref. [24], the $Z = 108$ shell gap is similar as that in the present work, while the energy gap at $N = 162$ is a bit smaller than ours.

3.3 One-dimensional potential energy curves of ^{270}Hs

In this subsection, we present the results of the MDC-RMF calculations with a constraint made on the axial quadrupole deformation β_{20} for ^{270}Hs . We examine one-dimensional (1D) PECs and discuss the influences of the axial octupole deformation β_{30} and non-axial quadrupole deformation β_{22} along these PECs. The (dis)continuities of these PECs are investigated in detail.

In the MDC-RMF model, both the triaxial (TA) and reflection asymmetric (RA) deformations are allowed. We may switch off TA or RA deformations and keep the nucleus in question to be axially symmetric (AS) or reflection symmetric (RS). Thus four typical combinations of symmetries can be imposed in the MDC-RMF calculations: AS-RS, AS-RA, TA-RS and TA-RA. In the 1D constraint calculations in the present work, we take β_{20} values running from 0 to 1.5 with the step size $\delta\beta_{20} = 0.02$ when $\beta_{20} < 1$. When $\beta_{20} > 1$, we take $\delta\beta_{20} = 0.02$ in AS-RS calculations and $\delta\beta_{20} = 0.05$ in the AS-RA, TA-RS and TA-RA calculations.

Four PECs of ^{270}Hs calculated from the MDC-RMF model are shown in Figure 2. These four PECs are identical in the following β_{20} intervals: $0 \leq \beta_{20} \leq 0.42$ and $0.88 \leq \beta_{20} \leq 1.50$. In particular, the global minimum corresponding to the ground state of ^{270}Hs coincides in all these four calculations regardless of the imposed symmetries. For the AS-RS PEC in Figure 2, the first fission barrier occurs at around $\beta_{20} = 0.46$ and the height of this barrier is 5.4 MeV. The second minimum in the AS-RS PEC occurs at $\beta_{20} = 0.52$ and the energy of this minimum is 4.8 MeV above the ground state. The depth of the pocket around the second minimum is about 0.6 MeV. The second fission barrier is around $\beta_{20} = 0.66$ with a height of 7.9 MeV. If the reflection asymmetry is considered, one gets the AS-RA PEC in which the height of the first barrier is 5.2 MeV, which is by 0.2 MeV lower than that in the AS-RS curve. The second minimum is shifted to $\beta_{20} = 0.54$ and the energy is by 0.1 MeV smaller than that from the reflection symmetric calculation. Though it does not affect the first barrier and the second minimum very much, the reflec-

tion asymmetric shape has a considerably large effect on the second fission barrier which is not only shifted to $\beta_{20} = 0.74$ but also lowered by 2.1 MeV (cf. violet and red curves in Figure 2). The TA-RS PEC is still of double-hump structure and the depth of the pocket around the second minimum is about 0.6 MeV. It can be seen that the triaxial distortion does not influence much the first barrier and the second minimum, but lowers the second fission barrier by about 2.4 MeV. This lowering effect is very pronounced considering that the height of the second barrier in the AS-RS PEC is only 7.9 MeV. The fact that the triaxiality affects much only the second fission barrier in ^{270}Hs is different from the findings in actinides in which the triaxial deformations lowers both the first and the second fission barriers considerably [37, 39]. When both triaxial and reflection asymmetric shapes are allowed in the MDC-RMF calculations, we obtain the TA-RA PEC which is shown in Figure 2 as black dots connected with a solid line. Compared with the TA-RS PEC, the TA-RA curve is slightly lower in the region $0.44 \leq \beta_{20} \leq 0.62$ as can be seen more clearly in the insets of Figure 2. We note that the RS PECs have been obtained for ^{270}Hs from Woods–Saxon–Strutinsky calculations in reflection symmetric deformation space (β_2, γ, β_4) [125].

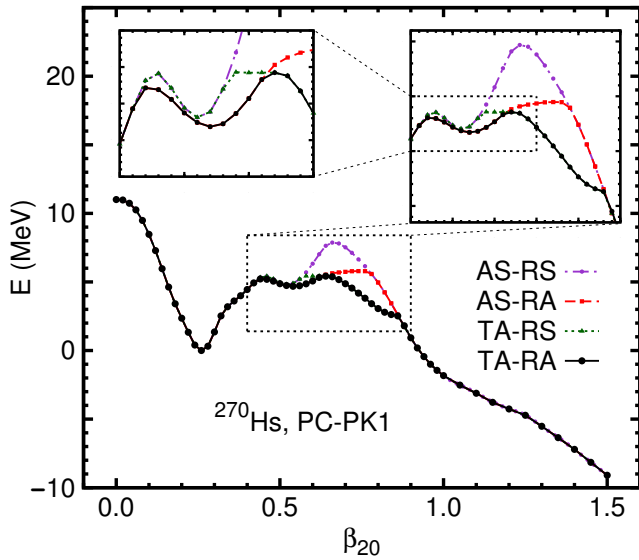


Figure 2 (Color online) Potential energy curves of ^{270}Hs obtained from MDC-RMF calculations with four combinations of symmetries imposed: axially symmetric and reflection symmetric (AS-RS) deformations, axially symmetric and reflection asymmetric (AS-RA) deformations, triaxial and reflection symmetric (TA-RS) deformations, and triaxial and reflection asymmetric (TA-RA) deformations. The inset on the top right shows these four PECs in the region $0.4 \leq \beta_{20} \leq 0.9$ beyond which the four curves are identical. The inset on the top left shows these PECs in the region $0.4 \leq \beta_{20} \leq 0.7$. Note that the TA-RS PEC overlaps with the TA-RA curve when $\beta_{20} \geq 0.64$ and the AS-RA and TA-RA PECs overlap with each other when $\beta_{20} \leq 0.62$.

In Figure 2, the energy is continuous as a function of β_{20}

along the four PECs. However, the $\beta_{30} \sim \beta_{20}$ and $\beta_{22} \sim \beta_{20}$ curves are discontinuous along the AS-RA, TA-RS and TA-RA PECs as shown in Figure 3 and Figure 4. In Figure 3, we can see that β_{30} keeps to be 0 when $0 \leq \beta_{20} \leq 0.42$, jumps to 0.14 at $\beta_{20} = 0.44$ and increases monotonically until $\beta_{20} = 0.76$ in the AS-RA curve. After a sudden drop at $\beta_{20} = 0.78$, β_{30} becomes 0 again. In the TA-RS PEC shown in Figure 4, β_{22} is 0 until $\beta_{20} = 0.56$. Then β_{22} jumps to 0.067 at $\beta_{20} = 0.58$ and changes continuously in the region $0.58 \leq \beta_{20} \leq 0.86$. At $\beta_{20} = 0.88$, β_{22} drops again to 0. As for the TA-RA PEC, since both triaxial and reflection asymmetric shapes are allowed, both β_{22} and β_{30} can be non-zero. It is seen that in Figure 3 there are sudden changes in β_{30} at $\beta_{20} = 0.44$ and $\beta_{20} = 0.64$ while in Figure 4 there are sudden changes in β_{22} at $\beta_{20} = 0.64$ and $\beta_{20} = 0.88$. Moreover, in the TA-RA PEC obtained by constraining only β_{20} , either β_{22} or β_{30} is 0 which means that the triaxial and octupole deformations do not co-exist. Note that in actinide nuclei the triaxial and octupole deformations do co-exist around the second fission barriers [37, 39].

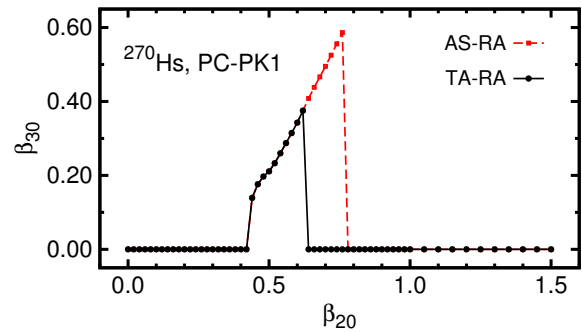


Figure 3 (Color online) Axial octupole deformation parameter β_{30} as a function of β_{20} along the axially symmetric and reflection asymmetric (AS-RA) and triaxial and reflection asymmetric (TA-RA) potential energy curves shown in Figure 2. Note that the two curves overlap with each other when $\beta_{20} \leq 0.62$ and $\beta_{20} \geq 0.78$.

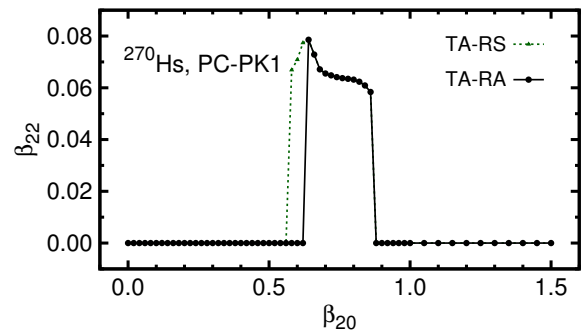


Figure 4 (Color online) Triaxial deformation parameter β_{22} as a function of β_{20} along the triaxial and reflection symmetric (TA-RS) and triaxial and reflection asymmetric (TA-RA) potential energy curves shown in Figure 2. Note that the two curves overlap with each other when $\beta_{20} \leq 0.56$ and $\beta_{20} \geq 0.64$.

These sudden changes of β_{30} or β_{22} in the AS-RA, TA-RS and TA-RA PECs come from the complexity of multidimensional PESs [39, 126, 127]. In the self-consistent calculations constraining only β_{20} , shape degrees of freedom other than β_{20} are minimized automatically in the process of finding (local) minima in a PES. It often happens that there are two or more valleys in a higher-dimensional PES. When such a PES is projected onto a lower-dimensional one, these valleys may overlap or be connected abruptly, resulting in “continuous” PESs (e.g., the AS-RA, TA-RS and TA-RA PECs in Figure 2) though the deformation parameters which are projected out may change suddenly at intersecting or connecting point(s) (e.g., β_{30} in Figure 3 or β_{22} in Figure 4). In fact, the AS-RA or TA-RS PECs shown in Figure 2 consist of three isolated curves in the two-dimensional PES; e.g., for the AS-RA PEC, the three parts correspond to the following three β_{20} intervals as seen in Figure 3: ($0 \leq \beta_{20} \leq 0.42$), ($0.44 \leq \beta_{20} \leq 0.76$) and ($0.78 \leq \beta_{20} \leq 1.50$). As seen in Figure 3 and Figure 4, the TA-RA PEC in Figure 2 consists of even four segments in the three-dimensional (3D) coordinate system with β_{20} , β_{22} , and β_{30} as coordinates: ($0 \leq \beta_{20} \leq 0.42$), ($0.44 \leq \beta_{20} \leq 0.62$), ($0.64 \leq \beta_{20} \leq 0.86$) and ($0.88 \leq \beta_{20} \leq 1.50$). The first and forth segments are along the β_{20} -axis ($\beta_{30} = 0, \beta_{22} = 0$), the second is in the β_{20} - β_{30} plane ($\beta_{30} \neq 0, \beta_{22} = 0$) and the third is in the β_{20} - β_{22} plane ($\beta_{30} = 0, \beta_{22} \neq 0$). It is clear that one needs to examine higher-dimensional PESs in order to eliminate such discontinuities.

3.4 Two-dimensional potential energy surfaces of ^{270}Hs

In this subsection, we present and discuss the two-dimensional (2D) PESs of ^{270}Hs which are obtained by simultaneously constraining the axial quadrupole deformation β_{20} and the axial octupole deformation β_{30} . In the 2D constraint calculations, we take β_{20} values running from 0.00 to 2.00 and β_{30} from 0.00 to 3.00, both with a step size of 0.02. One certainly does not need to calculate all points on this deformation lattice thus defined. The points in the top left corner of the PES with energy larger than 16 MeV (relative to the ground state) and those in the bottom right corner with energy lower than the ground state are not calculated.

The 2D PES for ^{270}Hs with the axial symmetry is shown in Figure 5. This PES is obtained from the MDC-RMF calculations with β_{20} and β_{30} constrained and the axial symmetry imposed. In Figure 5, one can find two valleys corresponding to two possible fission paths. One of them goes along the axis of abscissas, i.e., ^{270}Hs keeps $\beta_{30} = 0$ when it is elongated along this fission path. The energy of ^{270}Hs is smaller than the ground state energy when $\beta_{20} \approx 0.9$. ^{270}Hs becomes very soft against β_{30} distortion for $\beta_{20} > 0.4$ where the other possible fission path appears along the reflection asymmetric

valley. The reflection asymmetric fission path extends much farther than the reflection symmetric one in the directions of both β_{20} and β_{30} and the energy goes below the ground state at $\beta_{20} \approx 1.96$ and $\beta_{30} \approx 2.7$. In Figure 5, the density profiles of ^{270}Hs corresponding to the two fission configurations are also shown. The two fragments in the symmetric fission can certainly be identified as ^{135}Xe . However, the fission along the RA path is extremely asymmetric: The heavy fragment corresponds to ^{208}Pb and the light one to ^{62}Fe . Such an asymmetric fission may be considered as cluster radioactivity caused by the strong shell effects in ^{208}Pb [128].

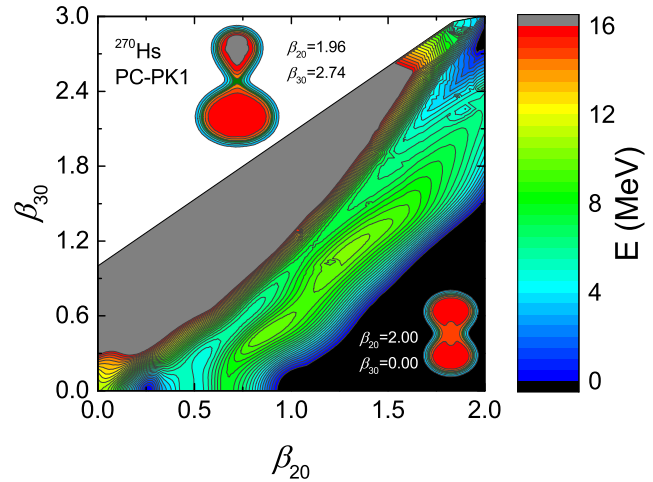


Figure 5 (Color online) Potential energy surface of ^{270}Hs obtained from 2D constraint RMF calculations with axial and reflection asymmetric (AS-RA) shapes allowed. The energy is normalized with respect to the binding energy of the ground state. The contour interval is 0.5 MeV. The density profiles of ^{270}Hs at $(\beta_{20} = 1.96, \beta_{30} = 2.74)$ and $(\beta_{20} = 2.00, \beta_{30} = 0.00)$ are shown.

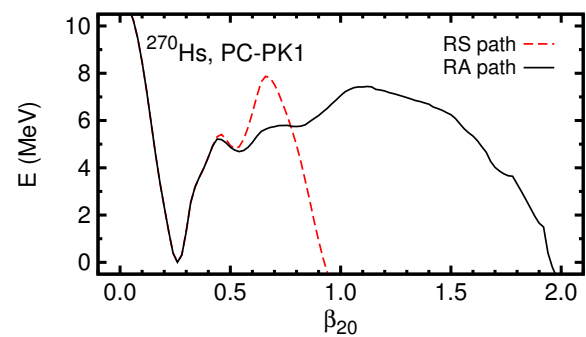


Figure 6 (Color online) Potential energy curves of ^{270}Hs corresponding to the reflection symmetric (RS) and reflection asymmetric (RA) fission paths in Figure 5. The energy is normalized with respect to the binding energy of the ground state. Note that the two curves overlap with each other when $\beta_{20} < 0.44$.

Along both paths, there are two or more minima and barriers which can be seen more clearly in Figure 6. The RS path in Figure 6 corresponds to the AS-RS PEC in Figure 2. At

$\beta_{20} = 0.78$ the RS and RA PECs cross in Figure 6. When $\beta_{20} \leq 0.76$, the RA PEC in Figure 6 is the same as the AS-RA PEC in Figure 2, while it is much higher than the latter when $\beta_{20} \geq 0.78$. The energy minimization in 1D constraint RMF calculations makes the AS-RA curve in Figure 2 follow the valley with the lowest energy which corresponds to the RS path with $\beta_{20} \geq 0.78$ in Figure 6. Only if 2D constraints on both β_{20} and β_{30} are made, one can stick to the reflection asymmetric path even though energies of some points in this path are not the lowest. Along the RA path, one can find a pocket around $\beta_{20} = 0.54$ ($\beta_{30} = 0.26$ as read in Figure 5) and a shoulder around $\beta_{20} = 0.80$ ($\beta_{30} = 0.64$). The highest barrier with a height 7.4 MeV is around $\beta_{20} = 1.12$ ($\beta_{30} = 1.18$), which is lower by about 0.5 MeV than the barrier around $\beta_{20} = 0.66$ in the RS path.

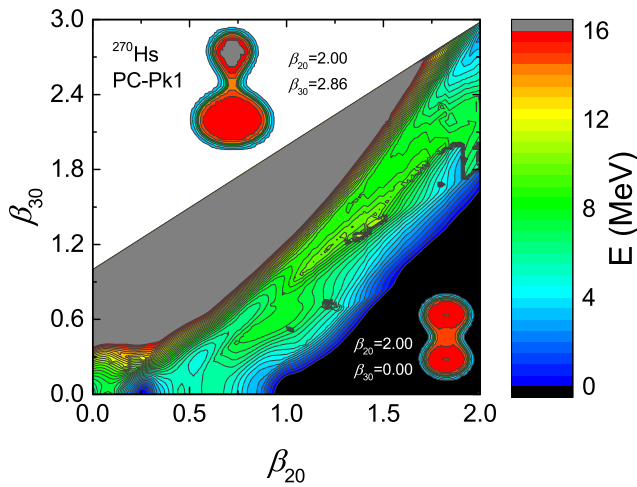


Figure 7 (Color online) Potential energy surface of ^{270}Hs obtained from 2D constraint RMF calculations with triaxial and reflection asymmetric (TA-RA) deformations allowed. The energy is normalized with respect to the binding energy of the ground state. The contour interval is 0.5 MeV. The density profiles of ^{270}Hs at $(\beta_{20} = 2.00, \beta_{30} = 2.86)$ and $(\beta_{20} = 2.00, \beta_{30} = 0)$ are shown.

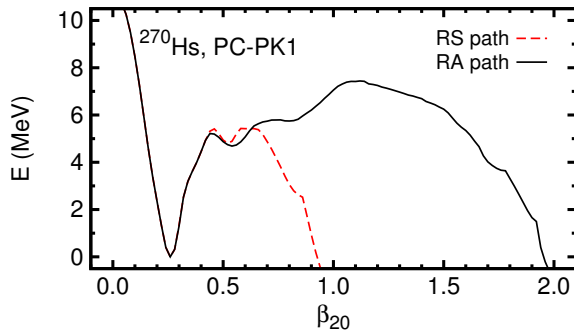


Figure 8 (Color online) Potential energy curves of ^{270}Hs corresponding to the reflection symmetric (RS) and reflection asymmetric (RA) fission paths in Figure 7 but recalculated with the ADHO basis truncated with $N_f = 20$. The energy is normalized with respect to the binding energy of the ground state. Note that the two curves overlap with each other when $\beta_{20} < 0.44$.

2D-constraint RMF calculations are carried out for ^{270}Hs with both triaxial and reflection asymmetric shapes allowed. The 2D PES thus obtained is shown in Figure 7. The TA PES shares some common features as the AS PES in Figure 5. There are also two competing fission paths, the RS path along the β_{20} -axis with $\beta_{30} = 0$ and the RA path going to the top right corner of this plot. In this PES, there are some discontinuities, e.g., around $(\beta_{20} \approx 1.2, \beta_{30} \approx 0.7)$, $(\beta_{20} \approx 1.5, \beta_{30} \approx 1.4)$ and $(\beta_{20} \approx 1.9, \beta_{30} \approx 1.8)$. These discontinuities may also be due to the complexity of multi-dimensional PES, similar to those in 1D PECs as shown in Figure 3 and Figure 4. To resolve these discontinuities, one has to investigate 3D PES by making 3D constraint calculations on β_{20}, β_{30} and β_{22} .

By comparing Figure 5 and Figure 7 and examining the β_{22} values of the points in the PES shown in Figure 7, it is found that the triaxial deformation is zero along the reflection asymmetric fission path. However, the triaxial effects are significant along the reflection symmetric fission path. In Figure 8, the PECs of ^{270}Hs corresponding to the RS and RA fission paths in Figure 7 are presented. To discuss quantitatively the influence of the triaxiality, these two curves are obtained from MDC-RMF calculations with the ADHO basis space truncated up to $N_f = 20$. In fact, the RA path in Figure 8 (the black curve) is the same as that in Figure 6 because ^{270}Hs does not favor a triaxial deformation along this path. Moreover, the RS PEC in Figure 8 is the same as the TA-RS PEC in Figure 2. In contrast with the RA path, the RS fission path is lowered considerably by the triaxial distortion. Compared to the RS path in Figure 6, the second barrier of the RS fission path in Figure 8 is lowered by 2.4 MeV. As a result, the fission barrier along the RS path is much lower than that in the RA path. Comparing Figure 2, Figure 6 and Figure 8, we finally come to the conclusion that the TA-RS PEC corresponds to the lowest static fission path though it is higher in energy than the TA-RA curve in Figure 2. Such a conclusion can only be reached when both 1D PECs and 2D PESs are examined carefully and when both triaxial and reflection asymmetric deformations are considered.

4 Summary and perspectives

We have investigated in detail the doubly magic deformed SHN ^{270}Hs with the MDC-RMF model. The successful effective interaction PC-PK1 is adopted for the covariant density functional and a separable pairing force of finite range is used in the pp channel. The binding energy, rms charge radius and deformation parameters obtained for the ground state of this nucleus are compared with predictions from other models and the empirical value in AME2016 and good agree-

ments are found. In single particle level schemes of protons and neutrons, there are relatively large shell gaps at $Z = 108$ and $N = 162$ which cause the deformed double magicity in ^{270}Hs .

If only 1D PECs are examined, one is easily led to a wrong static fission path which is, though the lowest in energy, very likely to be discontinuous in 2D or higher-dimensional PESs. Therefore we investigate in detail 1D PECs and 2D PESs with various spatial symmetries imposed. We stress that it is for the first time the PES is presented for ^{270}Hs with both triaxiality and reflection asymmetry considered. When the axial symmetry is assumed, the reflection asymmetric fission barrier is lower than the reflection symmetric one. When the triaxial deformation is allowed, the reflection symmetric fission path becomes favorable because the reflection symmetric barrier is lowered very much by the triaxial distortion. Although it is higher than the reflection symmetric one, the reflection asymmetric fission barrier may still be penetrated or overcome by ^{270}Hs in spontaneous or induced fissions. If this happens, ^{270}Hs would end with fragments with very large mass asymmetry, ^{208}Pb and ^{62}Fe , which may be considered as cluster emission resulted from the strong shell effects.

The above conclusions will be useful for learning detailed information about PESs and fission barrier properties of SHN. Furthermore, as the first thorough study on SHN with the MDC-RMF model, this work serves as the starting point of systematic investigations of SHN with MDC-CDFTs. In the future, more efforts will be devoted to the calculations of TA-RA PESs with larger N_f and 3D PESs, systematic studies of static fission paths and fission barriers of SHN, investigations of fission dynamics based on the PESs from MDC-CDFTs and cluster radioactivity, etc.

We thank Zhong-Ming Niu for allowing us to use the results for ^{270}Hs in Ref. [108] prior to publication and discussions concerning nuclear binding energy and mass excess. This work was supported by the National Key R&D Program of China (Grant No. 2018YFA0404402), the National Natural Science Foundation of China (Grants No. 11525524, No. 11621131001, No. 11647601, No. 11747601, and No. 11711540016), the Key Research Program of Frontier Sciences of Chinese Academy of Sciences (No. QYZDB-SSWSYS013), the Key Research Program of Chinese Academy of Sciences (No. XDPB09-02), the Inter-Governmental S&T Cooperation Project between China and Croatia, and the IAEA Coordinated Research Project "F41033". The results described in this paper are obtained on the High-performance Computing Cluster of KLTP/ITP-CAS and the ScGrid of the Supercomputing Center, Computer Network Information Center of Chinese Academy of Sciences.

Conflict of interest The authors declare that they have no conflict of interest.

- 1 J. Hamilton, S. Hofmann, Y. Oganessian, Search for superheavy nuclei, *Annu. Rev. Nucl. Part. Sci.* 63 (1) (2013) 383–405.
URL <https://doi.org/10.1146/annurev-nucl-102912-144535>
- 2 W. Nazarewicz, The limits of nuclear mass and charge, *Nat. Phys.* 14 (6) (2018) 537–541.

- URL <https://doi.org/10.1038/s41567-018-0163-3>
- 3 S. A. Giuliani, Z. Matheson, W. Nazarewicz, E. Olsen, P.-G. Reinhard, J. Sadhukhan, B. Schuetrumpf, N. Schunck, P. Schwerdtfeger, Colloquium: Superheavy elements: Oganesson and beyond, *Rev. Mod. Phys.* 91 (1) (2019) 011001–25.
URL <https://doi.org/10.1103/RevModPhys.91.011001>
- 4 W. D. Myers, W. J. Swiatecki, Nuclear masses and deformations, *Nucl. Phys.* 81 (1) (1966) 1–60.
URL [https://doi.org/10.1016/0029-5582\(66\)90639-0](https://doi.org/10.1016/0029-5582(66)90639-0)
- 5 C. Y. Wong, Additional evidence of stability of the superheavy element $^{310}126$ according to the shell model, *Phys. Lett.* 21 (6) (1966) 688–690.
URL [https://doi.org/10.1016/0031-9163\(66\)90127-2](https://doi.org/10.1016/0031-9163(66)90127-2)
- 6 A. Sobiczewski, F. Gareev, B. Kalinkin, Closed shells for $Z > 82$ and $N > 126$ in a diffuse potential well, *Phys. Lett.* 22 (4) (1966) 500–502.
URL [https://doi.org/10.1016/0031-9163\(66\)91243-1](https://doi.org/10.1016/0031-9163(66)91243-1)
- 7 H. Meldner, Predictions of new magic regions and masses for superheavy nuclei from calculations with realistic shell model single particle Hamiltonian, *Ark. Fys.* 36 (2) (1967) 593–598.
- 8 U. Mosel, W. Greiner, On the stability of superheavy nuclei against fission, *Z. Phys.* 222 (3) (1969) 261–282.
URL <https://doi.org/10.1007/BF01392125>
- 9 S. G. Nilsson, C. F. Tsang, A. Sobiczewski, Z. Szymanski, S. Wycech, C. Gustafson, I.-L. Lamm, P. Möller, B. Nilsson, On the nuclear structure and stability of heavy and superheavy elements, *Nucl. Phys. A* 131 (1) (1969) 1–66.
URL [https://doi.org/10.1016/0375-9474\(69\)90809-4](https://doi.org/10.1016/0375-9474(69)90809-4)
- 10 S. Hofmann, G. Münzenberg, The discovery of the heaviest elements, *Rev. Mod. Phys.* 72 (3) (2000) 733–767.
URL <https://doi.org/10.1103/RevModPhys.72.733>
- 11 K. Morita, SHE research at RIKEN/GARIS, *Nucl. Phys. A* 944 (2015) 30–61.
URL <https://doi.org/10.1016/j.nuclphysa.2015.10.007>
- 12 Y. T. Oganessian, A. Sobiczewski, G. M. Ter-Akopian, Superheavy nuclei: from predictions to discovery, *Phys. Scr.* 92 (2) (2017) 023003–21.
URL <https://doi.org/10.1088/1402-4896/aa53c1>
- 13 K. Rutz, M. Bender, T. Burvenich, T. Schilling, P.-G. Reinhard, J. A. Maruhn, W. Greiner, Superheavy nuclei in self-consistent nuclear calculations, *Phys. Rev. C* 56 (1) (1997) 238–243.
URL <https://doi.org/10.1103/PhysRevC.56.238>
- 14 W. Zhang, J. Meng, S. Zhang, L. Geng, H. Toki, Magic numbers for superheavy nuclei in relativistic continuum Hartree-Bogoliubov theory, *Nucl. Phys. A* 753 (1-2) (2005) 106–135.
URL <https://doi.org/10.1016/j.nuclphysa.2005.02.086>
- 15 A. Sobiczewski, K. Pomorski, Description of structure and properties of superheavy nuclei, *Prog. Part. Nucl. Phys.* 58 (1) (2007) 292–349.
URL <https://doi.org/10.1016/j.pnpnp.2006.05.001>
- 16 X.-R. Zhou, C. Qiu, H. Sagawa, Effect of tensor interaction on the shell structure of superheavy nuclei, in: H.-B. Bai, J. Meng, E.-G. Zhao, S.-G. Zhou (Eds.), *Nuclear Structure in China 2010 — Proceedings of the 13th National Conference on Nuclear Structure in China*, Chi-Feng, Inner Mongolia, China, 24 C 30 July 2010, World Scientific, 2011, pp. 259–267.
URL https://doi.org/10.1142/9789814360654_0046
- 17 J. J. Li, W. H. Long, J. Margueron, N. Van Giai, Superheavy magic structures in the relativistic Hartree-Fock-Bogoliubov approach, *Phys. Lett. B* 732 (2014) 169–173.
URL <https://doi.org/10.1016/j.physletb.2014.03.031>
- 18 Q. Mo, M. Liu, N. Wang, Systematic study of shell gaps in nuclei, *Phys. Rev. C* 90 (2) (2014) 024320–8.
URL <https://doi.org/10.1103/PhysRevC.90.024320>
- 19 A. Afanasjev, S. Agbemava, A. Gyawali, Hyperheavy nuclei: Existence and stability, *Phys. Lett. B* 782 (2018) 533–540.

- URL <https://doi.org/10.1016/j.physletb.2018.05.070>
- 20 S. E. Agbemava, A. V. Afanasjev, A. Taninah, A. Gyawali, Extension of the nuclear landscape to hyperheavy nuclei, *Phys. Rev. C* 99 (3) (2019) 034316–26.
URL <https://doi.org/10.1103/PhysRevC.99.034316>
- 21 P. Möller, S. G. Nilsson, J. R. Nix, Calculated ground-state properties of heavy nuclei, *Nucl. Phys. A* 229 (2) (1974) 292–319.
URL [https://doi.org/10.1016/0375-9474\(74\)90789-1](https://doi.org/10.1016/0375-9474(74)90789-1)
- 22 S. Ćwiok, V. V. Pashkevich, J. Dudek, W. Nazarewicz, Fission barriers of transfermium elements, *Nucl. Phys. A* 410 (2) (1983) 254–270.
URL [https://doi.org/10.1016/0375-9474\(83\)90201-4](https://doi.org/10.1016/0375-9474(83)90201-4)
- 23 Z. Patyk, J. Skalski, A. Sobczewski, S. Ćwiok, Potential energy and spontaneous-fission half-lives for heavy and superheavy nuclei, *Nucl. Phys. A* 502 (1989) 591–600.
URL [https://doi.org/10.1016/0375-9474\(89\)90691-x](https://doi.org/10.1016/0375-9474(89)90691-x)
- 24 Z. Patyk, A. Sobczewski, Ground-state properties of the heaviest nuclei analyzed in a multidimensional deformation space, *Nucl. Phys. A* 533 (1) (1991) 132–152.
URL [http://dx.doi.org/10.1016/0375-9474\(91\)90823-O](http://dx.doi.org/10.1016/0375-9474(91)90823-O)
- 25 R. Smolanczuk, J. Skalski, A. Sobczewski, Spontaneous-fission half-lives of deformed superheavy nuclei, *Phys. Rev. C* 52 (4) (1995) 1871–1880.
URL <https://doi.org/10.1103/PhysRevC.52.1871>
- 26 J. Dvorak, W. Brühlle, M. Chelnokov, R. Dressler, C. E. Düllmann, K. Eberhardt, V. Gorshkov, E. Jäger, R. Krücken, A. Kuznetsov, Y. Nagame, F. Nebel, Z. Novackova, Z. Qin, M. Schädel, B. Schausten, E. Schimpf, A. Semchenkov, P. Thörle, A. Türler, M. Wegrzecki, B. Wierczinski, A. Yakushev, A. Yeremin, Doubly magic nucleus $^{270}_{108}\text{Hs}_{162}$, *Phys. Rev. Lett.* 97 (24) (2006) 242501–4.
URL <https://doi.org/10.1103/PhysRevLett.97.242501>
- 27 Y. T. Oganessian, V. K. Utyonkov, F. S. Abdullin, S. N. Dmitriev, R. Graeger, R. A. Henderson, M. G. Itkis, Y. V. Lobanov, A. N. Mezentsev, K. J. Moody, S. L. Nelson, A. N. Polyakov, M. A. Ryabinin, R. N. Sagaidak, D. A. Shaughnessy, I. V. Shirokovsky, M. A. Stoyer, N. J. Stoyer, V. G. Subbotin, K. Subotic, A. M. Sukhov, Y. S. Tsyganov, A. Türler, A. A. Voinov, G. K. Vostokin, P. A. Wilk, A. Yakushev, Synthesis and study of decay properties of the doubly magic nucleus ^{270}Hs in the $^{226}\text{Ra} + ^{48}\text{Ca}$ reaction, *Phys. Rev. C* 87 (3) (2013) 034605–8.
URL <https://doi.org/10.1103/PhysRevC.87.034605>
- 28 V. V. Pashkevich, The energy of non-axial deformation of heavy nuclei, *Nucl. Phys. A* 133 (2) (1969) 400–404.
URL [https://doi.org/10.1016/0375-9474\(69\)90641-1](https://doi.org/10.1016/0375-9474(69)90641-1)
- 29 P. Möller, J. R. Nix, Calculation of fission barriers, in: *Proceedings of the Third IAEA Symposium on Physics and Chemistry of Fission*, Rochester, New York, 13–17 August 1973, Vol. 1, International Atomic Energy Agency, Vienna, 1974, pp. 103–140.
URL <https://www.nds.iaea.org/publications/item.php?key=STI-PUB-347V1>
- 30 K. Rutz, J. A. Maruhn, P. G. Reinhard, W. Greiner, Fission barriers and asymmetric ground states in the relativistic mean-field theory, *Nucl. Phys. A* 590 (3–4) (1995) 680–702.
URL [https://doi.org/10.1016/0375-9474\(95\)00192-4](https://doi.org/10.1016/0375-9474(95)00192-4)
- 31 L. M. Robledo, M. Warda, Cluster radioactivity of Th isotopes in the mean-field HFB theory, *Int. J. Mod. Phys. E* 17 (1) (2008) 204–211.
URL <https://doi.org/10.1142/S0218301308009707>
- 32 M. Kowal, P. Jachimowicz, A. Sobczewski, Fission barriers for even-even superheavy nuclei, *Phys. Rev. C* 82 (1) (2010) 014303–10.
URL <https://doi.org/10.1103/PhysRevC.82.014303>
- 33 Z. P. Li, T. Nikšić, D. Vretenar, P. Ring, J. Meng, Relativistic energy density functionals: Low-energy collective states of ^{240}Pu and ^{166}Er , *Phys. Rev. C* 81 (6) (2010) 064321–13.
URL <https://doi.org/10.1103/PhysRevC.81.064321>
- 34 H. Abusara, A. V. Afanasjev, P. Ring, Fission barriers in actinides in covariant density functional theory: The role of triaxiality, *Phys. Rev. C* 82 (4) (2010) 044303–11.
URL <https://doi.org/10.1103/PhysRevC.82.044303>
- 35 A. Staszczak, A. Baran, W. Nazarewicz, Breaking of axial and reflection symmetries in spontaneous fission of fermium isotopes, *Int. J. Mod. Phys. E* 20 (02) (2011) 552–556.
URL <https://doi.org/10.1142/S0218301311017995>
- 36 G. Royer, M. Jaffre, D. Moreau, Fission barriers and half-lives of actinides in the quasimolecular shape valley, *Phys. Rev. C* 86 (4) (2012) 044326–7.
URL <https://doi.org/10.1103/PhysRevC.86.044326>
- 37 B.-N. Lu, E.-G. Zhao, S.-G. Zhou, Potential energy surfaces of actinide nuclei from a multidimensional constrained covariant density functional theory: Barrier heights and saddle point shapes, *Phys. Rev. C* 85 (1) (2012) 011301(R)–5.
URL <https://doi.org/10.1103/PhysRevC.85.011301>
- 38 M. Warda, J. L. Egido, Fission half-lives of superheavy nuclei in a microscopic approach, *Phys. Rev. C* 86 (1) (2012) 014322–24.
URL <https://doi.org/10.1103/PhysRevC.86.014322>
- 39 B.-N. Lu, J. Zhao, E.-G. Zhao, S.-G. Zhou, Multidimensionally-constrained relativistic mean-field models and potential-energy surfaces of actinide nuclei, *Phys. Rev. C* 89 (1) (2014) 014323–15.
URL <https://doi.org/10.1103/PhysRevC.89.014323>
- 40 S.-G. Zhou, Multidimensionally constrained covariant density functional theories—nuclear shapes and potential energy surfaces, *Phys. Scr.* 91 (6) (2016) 063008–21.
URL <https://doi.org/10.1088/0031-8949/91/6/063008>
- 41 J. Zhao, B.-N. Lu, E.-G. Zhao, S.-G. Zhou, Tetrahedral shapes of neutron-rich Zr isotopes from a multidimensionally constrained relativistic Hartree-Bogoliubov model, *Phys. Rev. C* 95 (1) (2017) 014320–16.
URL <https://doi.org/10.1103/PhysRevC.95.014320>
- 42 B. D. Serot, J. D. Walecka, The relativistic nuclear many-body problem, *Adv. Nucl. Phys.* 16 (1986) 1–327.
- 43 P. G. Reinhard, The relativistic mean-field description of nuclei and nuclear dynamics, *Rep. Prog. Phys.* 52 (4) (1989) 439–514.
URL <https://doi.org/10.1088/0034-4885/52/4/002>
- 44 P. Ring, Relativistic mean field theory in finite nuclei, *Prog. Part. Nucl. Phys.* 37 (1996) 193–263.
URL [https://doi.org/10.1016/0146-6410\(96\)00054-3](https://doi.org/10.1016/0146-6410(96)00054-3)
- 45 M. Bender, P.-H. Heenen, P.-G. Reinhard, Self-consistent mean-field models for nuclear structure, *Rev. Mod. Phys.* 75 (1) (2003) 121–180.
URL <https://doi.org/10.1103/RevModPhys.75.121>
- 46 D. Vretenar, A. V. Afanasjev, G. A. Lalazissis, P. Ring, Relativistic Hartree-Bogoliubov theory: Static and dynamic aspects of exotic nuclear structure, *Phys. Rep.* 409 (3–4) (2005) 101–259.
URL <https://doi.org/10.1016/j.physrep.2004.10.001>
- 47 J. Meng, H. Toki, S. G. Zhou, S. Q. Zhang, W. H. Long, L. S. Geng, Relativistic continuum Hartree Bogoliubov theory for ground-state properties of exotic nuclei, *Prog. Part. Nucl. Phys.* 57 (2) (2006) 470–563.
URL <https://doi.org/10.1016/j.pnnp.2005.06.001>
- 48 N. Paar, D. Vretenar, G. Colo, Exotic modes of excitation in atomic nuclei far from stability, *Rep. Prog. Phys.* 70 (5) (2007) 691–793.
URL <https://doi.org/10.1088/0034-4885/70/5/R02>
- 49 T. Nikšić, D. Vretenar, P. Ring, Relativistic nuclear energy density functionals: Mean-field and beyond, *Prog. Part. Nucl. Phys.* 66 (3) (2011) 519–548.
URL <https://doi.org/10.1016/j.pnnp.2011.01.055>
- 50 H. Liang, J. Meng, S.-G. Zhou, Hidden pseudospin and spin symmetries and their origins in atomic nuclei, *Phys. Rep.* 570 (2015) 1–84.
URL <https://doi.org/10.1016/j.physrep.2014.12.005>
- 51 J. Meng, S. G. Zhou, Halos in medium-heavy and heavy nuclei with covariant density functional theory in continuum, *J. Phys. G: Nucl.*

- Part. Phys. 42 (9) (2015) 093101–52.
URL <https://doi.org/10.1088/0954-3899/42/9/093101>
- 52 J. Meng (Ed.), *Relativistic Density Functional for Nuclear Structure*, Vol. 10 of *International Review of Nuclear Physics*, World Scientific Pub Co Pte Lt, 2016.
URL <https://doi.org/10.1142/9872>
- 53 Y. K. Gambhir, P. Ring, A. Thimet, Relativistic mean field theory for finite nuclei, *Ann. Phys. (NY)* 198 (1) (1990) 132–179.
URL [https://doi.org/10.1016/0003-4916\(90\)90330-Q](https://doi.org/10.1016/0003-4916(90)90330-Q)
- 54 P. Ring, Y. K. Gambhir, G. A. Lalazissis, Computer program for the relativistic mean field description of the ground state properties of even-even axially deformed nuclei, *Comput. Phys. Commun.* 105 (1) (1997) 77–97.
URL [https://doi.org/10.1016/S0010-4655\(97\)00022-2](https://doi.org/10.1016/S0010-4655(97)00022-2)
- 55 A. V. Afanasjev, P. Ring, J. König, Cranked relativistic Hartree-Bogoliubov theory: formalism and application to the superdeformed bands in the $A = 190$ region, *Nucl. Phys. A* 676 (1-4) (2000) 196–244.
URL [https://doi.org/10.1016/S0375-9474\(00\)00187-1](https://doi.org/10.1016/S0375-9474(00)00187-1)
- 56 L.-S. Geng, J. Meng, H. Toki, Reflection asymmetric relativistic mean field approach and its application to the octupole deformed nucleus ^{226}Ra , *Chin. Phys. Lett.* 24 (7) (2007) 1865–1868.
URL <https://doi.org/10.1088/0256-307X/24/7/021>
- 57 W. Zhang, Z. P. Li, S. Q. Zhang, J. Meng, Octupole degree of freedom for the critical-point candidate nucleus ^{152}Sm in a reflection-asymmetric relativistic mean-field approach, *Phys. Rev. C* 81 (3) (2010) 034302–6.
URL <https://doi.org/10.1103/PhysRevC.81.034302>
- 58 Y. Wang, Z. Ren, Single particles in a reflection-asymmetric potential, *Sci. China-Phys. Mech. Astron.* 61 (8) (2018) 082012–8.
URL <https://doi.org/10.1007/s11433-018-9213-7>
- 59 B. Qi, H. Jia, C. Liu, S. Wang, Candidate chiral nuclei in bromine isotopes based on triaxial relativistic mean field theory, *Sci. China-Phys. Mech. Astron.* 62 (1) (2019) 012012–7.
URL <https://doi.org/10.1007/s11433-018-9265-6>
- 60 H. Xia, X. Wu, H. Mei, J. Yao, Beyond mean-field approach for pear-shaped hypernuclei, *Sci. China-Phys. Mech. Astron.* 62 (4) (2019) 042001–8.
URL <https://doi.org/10.1007/s11433-018-9308-0>
- 61 M. Warda, J. L. Egido, L. M. Robledo, K. Pomorski, Self-consistent calculations of fission barriers in the Fm region, *Phys. Rev. C* 66 (1) (2002) 014310–11.
URL <https://doi.org/10.1103/PhysRevC.66.014310>
- 62 S. Karatzikos, A. V. Afanasjev, G. A. Lalazissis, P. Ring, The fission barriers in Actinides and superheavy nuclei in covariant density functional theory, *Phys. Lett. B* 689 (2-3) (2010) 72–81.
URL <https://doi.org/10.1016/j.physletb.2010.04.045>
- 63 Y. Tian, Z.-Y. Ma, A separable pairing force in nuclear matter, *Chin. Phys. Lett.* 23 (12) (2006) 3226–3229.
URL <https://doi.org/10.1088/0256-307X/23/12/029>
- 64 Y. Tian, Z. Y. Ma, P. Ring, A finite range pairing force for density functional theory in superfluid nuclei, *Phys. Lett. B* 676 (1-3) (2009) 44–50.
URL <https://doi.org/10.1016/j.physletb.2009.04.067>
- 65 Y. Tian, Z.-y. Ma, P. Ring, Separable pairing force for relativistic quasiparticle random-phase approximation, *Phys. Rev. C* 79 (6) (2009) 064301–7.
URL <https://doi.org/10.1103/PhysRevC.79.064301>
- 66 P. Ring, P. Schuck, *The Nuclear Many-Body Problem*, Springer-Verlag, Berlin/Heidelberg/New York, 1980.
URL <https://www.springer.com/us/book/9783540212065>
- 67 J. Zhao, B.-N. Lu, D. Vretenar, E.-G. Zhao, S.-G. Zhou, Multidimensionally constrained relativistic mean-field study of triple-humped barriers in actinides, *Phys. Rev. C* 91 (1) (2015) 014321–9.
URL <https://doi.org/10.1103/PhysRevC.91.014321>
- 68 J. Zhao, B.-N. Lu, E.-G. Zhao, S.-G. Zhou, Nonaxial-octupole Y_{32} correlations in $N=150$ isotones from multidimensional constrained covariant density functional theories, *Phys. Rev. C* 86 (5) (2012) 057304–4.
URL <https://doi.org/10.1103/PhysRevC.86.057304>
- 69 C. Liu, S. Y. Wang, R. A. Bark, S. Q. Zhang, J. Meng, B. Qi, P. Jones, S. M. Wyngaardt, J. Zhao, C. Xu, S.-G. Zhou, S. Wang, D. P. Sun, L. Liu, Z. Q. Li, N. B. Zhang, H. Jia, X. Q. Li, H. Hua, Q. B. Chen, Z. G. Xiao, H. J. Li, L. H. Zhu, T. D. Bucher, T. Dinoko, J. Easton, K. Juhász, A. Kamblawe, E. Khaleel, N. Khumalo, E. A. Lawrie, J. J. Lawrie, S. N. T. Majola, S. M. Mullins, S. Murray, J. Ndayishimye, D. Negi, S. P. Noncolela, S. S. Ntshangase, B. M. Nyakó, J. N. Orce, P. Papka, J. F. Sharpey-Schafer, O. Shirinda, P. Sithole, M. A. Stankiewicz, M. Wiedeking, Evidence for octupole correlations in multiple chiral doublet bands, *Phys. Rev. Lett.* 116 (11) (2016) 112501–6.
URL <https://doi.org/10.1103/PhysRevLett.116.112501>
- 70 X. C. Chen, J. Zhao, C. Xu, H. Hua, T. M. Shneidman, S. G. Zhou, X. G. Wu, X. Q. Li, S. Q. Zhang, Z. H. Li, W. Y. Liang, J. Meng, F. R. Xu, B. Qi, Y. L. Ye, D. X. Jiang, Y. Y. Cheng, C. He, J. J. Sun, R. Han, C. Y. Niu, C. G. Li, P. J. Li, C. G. Wang, H. Y. Wu, Z. H. Li, H. Zhou, S. P. Hu, H. Q. Zhang, G. S. Li, C. Y. He, Y. Zheng, C. B. Li, H. W. Li, Y. H. Wu, P. W. Luo, J. Zhong, Evolution of octupole correlations in ^{123}Ba , *Phys. Rev. C* 94 (2) (2016) 021301(R)–5.
URL <https://doi.org/10.1103/PhysRevC.94.021301>
- 71 B.-N. Lu, E.-G. Zhao, S.-G. Zhou, Quadrupole deformation (β, γ) of light Λ hypernuclei in a constrained relativistic mean field model: Shape evolution and shape polarization effect of the Λ hyperon, *Phys. Rev. C* 84 (1) (2011) 014328–10.
URL <https://doi.org/10.1103/PhysRevC.84.014328>
- 72 B.-N. Lu, E. Hiyama, H. Sagawa, S.-G. Zhou, Superdeformed Λ hypernuclei within relativistic mean field models, *Phys. Rev. C* 89 (04) (2014) 044307–7.
URL <https://doi.org/10.1103/PhysRevC.89.044307>
- 73 J. Zhao, B.-N. Lu, T. Nikšić, D. Vretenar, Multidimensionally constrained relativistic Hartree-Bogoliubov study of spontaneous nuclear fission, *Phys. Rev. C* 92 (6) (2015) 064315–12.
URL <https://doi.org/10.1103/PhysRevC.92.064315>
- 74 J. Zhao, B.-N. Lu, T. Nikšić, D. Vretenar, S.-G. Zhou, Multidimensionally-constrained relativistic mean-field study of spontaneous fission: Coupling between shape and pairing degrees of freedom, *Phys. Rev. C* 93 (4) (2016) 044315–9.
URL <https://doi.org/10.1103/PhysRevC.93.044315>
- 75 J. Zhao, T. Nikšić, D. Vretenar, S.-G. Zhou, Microscopic self-consistent description of induced fission dynamics: Finite-temperature effects, *Phys. Rev. C* 99 (1) (2019) 014618–8.
URL <https://doi.org/10.1103/PhysRevC.99.014618>
- 76 J. Zhao, J. Xiang, Z.-P. Li, T. Nikšić, D. Vretenar, S.-G. Zhou, Time-dependent generator coordinate method study of mass-asymmetric fission of actinides, arXiv:1902.09535 [nucl-th] (Feb. 2019).
URL <https://arxiv.org/abs/1902.09535>
- 77 P. W. Zhao, Z. P. Li, J. M. Yao, J. Meng, New parametrization for the nuclear covariant energy density functional with a point-coupling interaction, *Phys. Rev. C* 82 (5) (2010) 054319–14.
URL <https://doi.org/10.1103/PhysRevC.82.054319>
- 78 P. Zhao, Z. Li, Spectroscopies of rod- and pear-shaped nuclei in covariant density functional theory, *Int. J. Mod. Phys. E* 27 (10) (2019) 1830007.
URL <https://doi.org/10.1142/S0218301318300072>
- 79 B. Sun, P. Zhao, J. Meng, Mass prediction of proton-rich nuclides with the Coulomb displacement energies in the relativistic point-coupling model, *Sci. China-Phys. Mech. Astron.* 54 (2) (2011) 210–214.
URL <http://dx.doi.org/10.1007/s11433-010-4222-8>
- 80 P. W. Zhao, L. S. Song, B. Sun, H. Geissel, J. Meng, Crucial test for

- covariant density functional theory with new and accurate mass measurements from Sn to Pa, *Phys. Rev. C* 86 (6) (2012) 064324–6.
URL <https://doi.org/10.1103/PhysRevC.86.064324>
- 81 K. Q. Lu, Z. X. Li, Z. P. Li, J. M. Yao, J. Meng, Global study of beyond-mean-field correlation energies in covariant energy density functional theory using a collective Hamiltonian method, *Phys. Rev. C* 91 (2) (2015) 027304–4.
URL <https://doi.org/10.1103/PhysRevC.91.027304>
- 82 X. W. Xia, Y. Lim, P. W. Zhao, H. Z. Liang, X. Y. Qu, Y. Chen, H. Liu, L. F. Zhang, S. Q. Zhang, Y. Kim, J. Meng, The limits of the nuclear landscape explored by the relativistic continuum Hartree-Bogoliubov theory, *At. Data Nucl. Data Tables* 121-122 (2018) 1–215.
URL <https://doi.org/10.1016/j.adt.2017.09.001>
- 83 P. W. Zhao, S. Q. Zhang, J. Meng, Explanation of the simplicity of the quadrupole moments recently observed in Cd isotopes from covariant density functional theory, *Phys. Rev. C* 89 (1) (2014) 011301(R)–5.
URL <https://doi.org/10.1103/PhysRevC.89.011301>
- 84 D. T. Jordanov, D. L. Balabanski, M. L. Bissell, K. Blaum, I. Budinčević, B. Cheal, K. Flanagan, N. Frömmgen, G. Georgiev, C. Geppert, M. Hammen, M. Kowalska, K. Kreim, A. Krieger, J. Meng, R. Neugart, G. Neyens, W. Nörtershäuser, M. M. Rajabali, J. Papuga, S. Schmidt, P. W. Zhao, Simple nuclear structure in $^{111-129}\text{Cd}$ from atomic isomer shifts, *Phys. Rev. Lett.* 116 (3) (2016) 032501–5.
URL <https://doi.org/10.1103/PhysRevLett.116.032501>
- 85 H. Haas, S. P. A. Sauer, L. Hemmingsen, V. Kellö, P. W. Zhao, Quadrupole moments of Cd and Zn nuclei: When solid-state, molecular, atomic, and nuclear theory meet, *EPL (Europhysics Letters)* 117 (6) (2017) 62001–6.
URL <https://doi.org/10.1209/0295-5075/117/62001>
- 86 S. Quan, Z. P. Li, D. Vretenar, J. Meng, Nuclear quantum shape-phase transitions in odd-mass systems, *Phys. Rev. C* 97 (3) (2018) 031301(R)–6.
URL <https://doi.org/10.1103/PhysRevC.97.031301>
- 87 P. W. Zhao, Multiple chirality in nuclear rotation: A microscopic view, *Phys. Lett. B* 773 (2017) 1–5.
URL <https://doi.org/10.1016/j.physletb.2017.08.001>
- 88 P. W. Zhao, S. Q. Zhang, J. Peng, H. Z. Liang, P. Ring, J. Meng, Novel structure for magnetic rotation bands in ^{60}Ni , *Phys. Lett. B* 699 (3) (2011) 181–186.
URL <https://doi.org/10.1016/j.physletb.2011.03.068>
- 89 P. W. Zhao, J. Peng, H. Z. Liang, P. Ring, J. Meng, Antimagnetic rotation band in nuclei: A microscopic description, *Phys. Rev. Lett.* 107 (12) (2011) 122501–5.
URL <https://doi.org/10.1103/PhysRevLett.107.122501>
- 90 J. Meng, J. Peng, S.-Q. Zhang, P.-W. Zhao, Progress on tilted axis cranking covariant density functional theory for nuclear magnetic and antimagnetic rotation, *Front. Phys.* 8 (1) (2013) 55–79.
URL <https://doi.org/10.1007/s11467-013-0287-y>
- 91 J. Peng, P. W. Zhao, Magnetic and antimagnetic rotation in ^{110}Cd within tilted axis cranking relativistic mean-field theory, *Phys. Rev. C* 91 (4) (2015) 044329–8.
URL <https://doi.org/10.1103/PhysRevC.91.044329>
- 92 J. Meng, P. Zhao, Nuclear chiral and magnetic rotation in covariant density functional theory, *Phys. Scr.* 91 (5) (2016) 053008–21.
URL <https://doi.org/10.1088/0031-8949/91/5/053008>
- 93 W. Zhang, Z. P. Li, S. Q. Zhang, Description of alpha-decay chains for $^{293,294}\text{117}$ within covariant density functional theory, *Phys. Rev. C* 88 (5) (2013) 054324–6.
URL <https://doi.org/10.1103/PhysRevC.88.054324>
- 94 S. E. Agbemava, A. V. Afanasjev, T. Nakatsukasa, P. Ring, Covariant density functional theory: Reexamining the structure of superheavy nuclei, *Phys. Rev. C* 92 (5) (2015) 054310–21.
URL <https://doi.org/10.1103/PhysRevC.92.054310>
- 95 Z.-X. Li, Z.-H. Zhang, P.-W. Zhao, Shape coexistence and alpha-decay chains of ^{293}Lv , *Front. Phys.* 10 (3) (2015) 268–275.
URL <https://doi.org/10.1007/s11467-015-0474-0>
- 96 Y. Tian, Z.-y. Ma, P. Ring, Axially deformed relativistic Hartree Bogoliubov theory with a separable pairing force, *Phys. Rev. C* 80 (2) (2009) 024313–7.
URL <https://doi.org/10.1103/PhysRevC.80.024313>
- 97 G. Audi, F. G. Kondev, M. Wang, W. J. Huang, S. Naimi, The NUBASE2016 evaluation of nuclear properties, *Chin. Phys. C* 41 (3) (2017) 030001–138.
URL <https://doi.org/10.1088/1674-1137/41/3/030001>
- 98 W. J. Huang, G. Audi, M. Wang, F. G. Kondev, S. Naimi, X. Xu, The AME2016 atomic mass evaluation (I). Evaluation of input data; and adjustment procedures, *Chin. Phys. C* 41 (3) (2017) 030002–344.
URL <https://doi.org/10.1088/1674-1137/41/3/030002>
- 99 M. Wang, G. Audi, F. G. Kondev, W. J. Huang, S. Naimi, X. Xu, The AME2016 atomic mass evaluation (II). Tables, graphs and references, *Chin. Phys. C* 41 (3) (2017) 030003–442.
URL <https://doi.org/10.1088/1674-1137/41/3/030003>
- 100 Z. Ren, Shape coexistence in even-even superheavy nuclei, *Phys. Rev. C* 65 (5) (2002) 051304(R)–5.
URL <https://doi.org/10.1103/PhysRevC.65.051304>
- 101 Z. Ren, F. Tai, D.-H. Chen, Systematic calculations of the ground state properties of superheavy nuclei, *Phys. Rev. C* 66 (6) (2002) 064306–13.
URL <https://doi.org/10.1103/PhysRevC.66.064306>
- 102 L. S. Geng, H. Toki, J. Meng, Masses, deformations and charge radii – nuclear ground-state properties in the relativistic mean field model, *Prog. Theo. Phys.* 113 (4) (2005) 785–800.
URL <https://doi.org/10.1143/PTP.113.785>
- 103 L. Geng, Ground state properties of finite nuclei in the relativistic mean field model, Ph.D. thesis, Osaka University (Mar. 2006).
- 104 S. Goriely, N. Chamel, J. M. Pearson, Further explorations of Skyrme-Hartree-Fock-Bogoliubov mass formulas. XIII. The 2012 atomic mass evaluation and the symmetry coefficient, *Phys. Rev. C* 88 (2) (2013) 024308–14.
URL <https://doi.org/10.1103/PhysRevC.88.024308>
- 105 H. F. Zhang, Y. Gao, N. Wang, J. Q. Li, E. G. Zhao, G. Royer, Double magic nuclei for $Z > 82$ and $N > 126$, *Phys. Rev. C* 85 (1) (2012) 014325–6.
URL <https://doi.org/10.1103/PhysRevC.85.014325>
- 106 N. Wang, M. Liu, X. Wu, J. Meng, Surface diffuseness correction in global mass formula, *Phys. Lett. B* 734 (0) (2014) 215–219.
URL <https://doi.org/10.1016/j.physletb.2014.05.049>
- 107 P. Möller, A. J. Sierk, T. Ichikawa, H. Sagawa, Nuclear ground-state masses and deformations: FRDM(2012), *At. Data Nucl. Data Tables* 109-110 (2016) 1–204.
URL <https://doi.org/10.1016/j.adt.2015.10.002>
- 108 M. Shi, Z. M. Niu, H. Z. Liang, Mass predictions of relativistic continuum Hartree-Bogoliubov model with radial basis function approach, *Chin. Phys. C*, in press.
- 109 N. Wang, M. Liu, X. Wu, Modification of nuclear mass formula by considering isospin effects, *Phys. Rev. C* 81 (4) (2010) 044322–8.
URL <https://doi.org/10.1103/PhysRevC.81.044322>
- 110 N. Wang, Z. Liang, M. Liu, X. Wu, Mirror nuclei constraint in nuclear mass formula, *Phys. Rev. C* 82 (4) (2010) 044304–6.
URL <https://doi.org/10.1103/PhysRevC.82.044304>
- 111 M. Liu, N. Wang, Y. Deng, X. Wu, Further improvements on a global nuclear mass model, *Phys. Rev. C* 84 (1) (2011) 014333–8.
URL <https://doi.org/10.1103/PhysRevC.84.014333>
- 112 J. Meng, P. Ring, Relativistic Hartree-Bogoliubov description of the neutron halo in ^{11}Li , *Phys. Rev. Lett.* 77 (19) (1996) 3963–3966.
URL <https://doi.org/10.1103/PhysRevLett.77.3963>
- 113 J. Meng, P. Ring, Giant halo at the neutron drip line, *Phys. Rev. Lett.* 80 (3) (1998) 460–463.
URL <https://doi.org/10.1103/PhysRevLett.80.460>

- 114 J. Meng, Relativistic continuum Hartree-Bogoliubov theory with both zero range and finite range Gogny force and their application, *Nucl. Phys. A* 635 (1-2) (1998) 3–42.
URL [https://doi.org/10.1016/S0375-9474\(98\)00178-X](https://doi.org/10.1016/S0375-9474(98)00178-X)
- 115 X. Qu, Y. Chen, S. Zhang, P. Zhao, I. Shin, Y. Lim, Y. Kim, J. Meng, Extending the nuclear chart by continuum: From oxygen to titanium, *Sci. China-Phys. Mech. Astron.* 56 (11) (2013) 2031–2036.
URL <https://doi.org/10.1007/s11433-013-5329-5>
- 116 M. D. Buhmann, *Radial Basis Functions*, Cambridge University Press, 2006.
- 117 N. Wang, M. Liu, Nuclear mass predictions with a radial basis function approach, *Phys. Rev. C* 84 (5) (2011) 051303(R)–4.
URL <https://doi.org/10.1103/PhysRevC.84.051303>
- 118 J. S. Zheng, N. Y. Wang, Z. Y. Wang, Z. M. Niu, Y. F. Niu, B. Sun, Mass predictions of the relativistic mean-field model with the radial basis function approach, *Phys. Rev. C* 90 (1) (2014) 014303–7.
URL <https://doi.org/10.1103/PhysRevC.90.014303>
- 119 Z. M. Niu, B. H. Sun, H. Z. Liang, Y. F. Niu, J. Y. Guo, Improved radial basis function approach with odd-even corrections, *Phys. Rev. C* 94 (5) (2016) 054315–7.
URL <https://doi.org/10.1103/PhysRevC.94.054315>
- 120 S.-G. Zhou, J. Meng, P. Ring, E.-G. Zhao, Neutron halo in deformed nuclei, *Phys. Rev. C* 82 (1) (2010) 011301(R)–5.
URL <https://doi.org/10.1103/PhysRevC.82.011301>
- 121 L. Li, J. Meng, P. Ring, E.-G. Zhao, S.-G. Zhou, Deformed relativistic Hartree-Bogoliubov theory in continuum, *Phys. Rev. C* 85 (2) (2012) 024312–17.
URL <https://doi.org/10.1103/PhysRevC.85.024312>
- 122 L. Li, J. Meng, P. Ring, E.-G. Zhao, S.-G. Zhou, Odd systems in deformed relativistic hartree bogoliubov theory in continuum, *Chin. Phys. Lett.* 29 (4) (2012) 042101–4.
URL <https://doi.org/10.1088/0256-307X/29/4/042101>
- 123 X.-X. Sun, J. Zhao, S.-G. Zhou, Shrunk halo and quenched shell gap at $N = 16$ in ^{22}C : Inversion of sd states and deformation effects, *Phys. Lett. B* 785 (2018) 530–535.
URL <https://doi.org/10.1016/j.physletb.2018.08.071>
- 124 The DRHBc Mass Table Collaboration, The limits of the nuclear landscape explored by the deformed relativistic Hartree-Bogoliubov model in continuum, in press.
- 125 Q.-Z. Chai, W.-J. Zhao, M.-L. Liu, H.-L. Wang, Calculation of multidimensional potential energy surfaces for even-even transuranium nuclei: systematic investigation of the triaxiality effect on the fission barrier, *Chin. Phys. C* 42 (5) (2018) 054101–11.
URL <https://doi.org/10.1088/1674-1137/42/5/054101>
- 126 P. Möller, A. J. Sierk, T. Ichikawa, A. Iwamoto, R. Bengtsson, H. Uhrenholt, S. Aberg, Heavy-element fission barriers, *Phys. Rev. C* 79 (6) (2009) 064304–38.
URL <https://doi.org/10.1103/PhysRevC.79.064304>
- 127 N. Dubray, D. Regnier, Numerical search of discontinuities in self-consistent potential energy surfaces, *Comput. Phys. Commun.* 183 (10) (2012) 2035–2041.
URL <https://doi.org/10.1016/j.cpc.2012.05.001>
- 128 Z. Matheson, S. A. Giuliani, W. Nazarewicz, J. Sadhukhan, N. Schunck, Cluster radioactivity of $^{294}_{118}\text{Og}_{176}$, arXiv:1812.06490 [nucl-th] (2018).
URL <https://arxiv.org/abs/1812.06490>